Guiral, A.; Alonso, A.; Baeza González, LM.; Giménez, J. (2013). Non-steady state modeling of wheel-rail contact problem. Vehicle System Dynamics. 51(1):91-108. doi:10.1080/00423114.2012.713499.

Non-steady state modeling of wheel-rail contact problem

A. Guiral, A. Alonso, L. Baeza, J.G. Giménez

Non-steady state modeling of wheel-rail contact problem
Vehicle System Dynamics, 51 (2013) 91-108.
http://dx.doi.org/10.1080/00423114.2012.713499

1. Notation

$s_\alpha(x,y,t)$	Relative wheel-rail slip velocity in α direction.
$u_\alpha(x,y,t)$	Relative tangential displacements between wheel and rail in α direction.
$w_\alpha(x,y,t)$	Rigid solid creepage in α direction.
$P_z(x,y,t)$	Normal pressure distribution on the contact area.
$\vec{\tau}(x,y,t)$	Tangential traction distribution.
V	Vehicle speed.
μ	Friction coefficient.
L	Flexibility coefficient.
L_s, L_v	Stationary and non-stationary flexibility coefficients.
a, b	Longitudinal and lateral semi-axes of the contact ellipse.
G	Shear modulus.
λ	Wavelength.
$\xi(t), \eta(t), \varphi(t)$	Longitudinal, lateral and spin time-dependent creepages.

2. Introduction

In railway vehicle dynamics the determination of the creep forces on the wheel-rail contact patch is of great importance. Railway simulation programs are required to solve the contact problem providing sufficiently accurate results with a low computational cost. The most extended theories used in these programs are Kalker's Linear Theory [1] and FastSim algorithm based on the Simplified Theory [2]. Both calculation methods are based on the assumption that the wavelength of the motion is large compared to the length of the contact area; this is, a stationary contact is assumed. However, in some cases this assumption is no longer valid. Among all, the following situations can be pointed out:

- Squeal noise on sharp curves.
- Rolling on rails with short wavelength irregularities (rolling noise).
- Vibration due to the flexibility of the wheelset-track system.
- Traction problems at the starting up.
- Development of short wavelength rail corrugation.

Non-stationary rolling contact mechanics was first addressed by Kalker [3], he did not studied it as such though, but as a transition from Cattaneo's solution [4] to Carter's solution [5]. Kalker was interested in determining the evolution of the stresses on the contact area when two identical bodies are compressed and rolled over each other [6]. It was not until 1986, when he published an exact theory known as Kalker's Variational Method [6], which came into fruition in CONTACT program. It is worth mentioning that this method converges towards the exact solution as the number of elements in which the contact path is discretized increases. In contrast, due to its high computational cost, its use is not appropriated for railway dynamics software and has been restricted to the validation of other contact theories.

The challenge of subsequent authors was, then, to develop a non-steady state theory suitable for its implementation in railway dynamics software. The objective was to reduce the computational cost of Kalker's Variational Method but assuring sufficiently accurate results.

One of the first works was carried out by Groß-Thebing [7], who centered his efforts in the extension of Kalker's Linear Theory into the high frequency range. Kalker's Linear Theory assumes that all the contact area is in adhesion condition and states a linear relationship between creepforces and creepages by means of the so known Kalker's coefficient. Gross-Thebing developed a methodology that allows calculating these coefficients in cases in which creepages vary harmonically at high frequency with small amplitudes – the reference state of all the creepages is zero. The coefficients calculated through this way result to be complex numbers indicating a phase difference between forces and creepages.

In a later work, Knothe and Groß-Thebing [8] extended this theory introducing the possibility of calculating the non-steady state Kalker's coefficients for non-zero creepage reference state.

Shen and Li [9] proposed a non-steady state algorithm based on Kalker's Simplified Theory of rolling contact. This method is a direct extension of FastSim algorithm to non-stationary contact mechanics in which the only modification consists in keeping the non-steady term of the slip equations. The non-steady state algorithm works for moderate values of the longitudinal creepage and for small pure spin. However, it has been demonstrated that, although the computational cost requirement is fulfilled, further work is needed in order to provide the sufficiently accurate results demanded by railway dynamics software.
Alonso and Giménez [10] also dealt with this problem. As Shen and Li, they took advantage of the success of FastSim and introduced the appropriated modifications with regard to the flexibility parameters demonstrating that accurate results could be obtained. This method is consequently able to give good results in a fast manner. However, it has two important limitations:

- The flexibility coefficients used in the non-steady state contact problem are obtained for situations in which only one of the creepages varies with time. Therefore, the accuracy when solving situations with different combinations of creepages is not handled.
- The method was developed for a constant normal load and its accuracy when a varying normal force exists has not been checked.

The aim of this paper is to present the required changes to extend the method of Alonso and Giménez so that these two disadvantages are overcome. A solution to deal with arbitrary combination of creepages will be presented and the accuracy of the results for variable normal load will be checked.
The contents of this paper are structured as follows: first the non-steady state FastSim of Alonso and Giménez will be introduced (Section 2). This section remarks the most significant steps to extend the stationary FastSim into the high frequency range and concludes with the presentation of some results. Afterwards, the proposed modifications of this algorithm will explained (Section 3). The first part of this section will deal with the use of the non-steady state FastSim for arbitrary combinations of creepages. A solution is suggested and checked for different amplitudes and frequencies of the creepages. The second part of this section evaluates the results of the method for variable normal loads. Moreover, in order to improve the efficiency of the algorithm a change in the discretization of the contact area will be proposed. Finally, some conclusions will be discussed.

3. Non-steady state contact problem theory of Alonso and Giménez

3.1. *Theory description*

Alonso and Giménez [10] worked on a non-stationary contact theory able to provide sufficiently accurate results with a low enough computational cost. This method is based on FastSim, and consequently on the Simplified Theory of Elasticity. In this theory, the tangential traction and deformation at each point of the contact area are related linearly through the flexibility parameter. Kalker obtained the value of the flexibility parameter comparing the stationary Simplified and Linear theories. Alonso and Giménez followed the same strategy for the non-stationary contact mechanics.

The general theory of the contact tangential problem states that, in order to calculate the tangential traction distribution, each point of the contact area should fulfilled the following slip equations:

$$s_\alpha(x,y,t) = w_\alpha(x,y,t) - \frac{\partial u_\alpha(x,y,t)}{\partial x} + \frac{1}{V}\cdot\frac{\partial u_\alpha(x,y,t)}{\partial t}. \quad (1)$$

Where,

- Subscript α (= x, y) denotes the direction of the slip,
- $s_\alpha(x,y,t)$ is the relative slip,
- $w_\alpha(x,y,t)$ is the rigid velocity,
- and $u_\alpha(x,y,t)$ is the displacement associated with the rail and wheel deformation.

The essential difference between a stationary and a non-stationary theory lies in the last term of equation (1), which refers to the temporal variation of the point deformation, $\partial u_\alpha(x,y,t)/\partial t$. In non-steady state contact mechanics this term acquires a significant influence and cannot be neglected.
In accordance to Coulomb's Law the tangential traction distribution at every point of the contact area must fulfil the following expression,

$$\left|\vec{\tau}(x,y,t)\right| \le \mu \cdot P_z(x,y,t). \quad (2)$$

To simplify the compression of this section, the friction coefficient, μ, is considered to be constant. To adapt the method for a slip-dependent friction law reference [11] can be consulted.

The relation between stresses and displacements is given by the theory of elasticity by means of Boussinesq-Cerruti equations. However, the determination of the exact solution of these equations is not computationally efficient. To avoid this difficulty, the simplified theory of elasticity is applied. According to this theory, the displacement at one point is directly proportional to the tangential stress at the same point through a proportionality parameter, L, known as flexibility coefficient.

$$\vec{u}(x,y,t) = L\cdot\vec{\tau}(x,y,t). \quad (3)$$

Substituting expression (3) in equation (1) and approximating the derivatives by means of finite differences, the relation between slip and the tangential traction is given as,

$$s_\alpha(x,y,t) = w_\alpha(x,y,t) - L\frac{\tau_\alpha(x+\Delta x,y,t)-\tau_\alpha(x,y,t)}{\Delta x} + \frac{L}{V}\cdot\frac{\tau_\alpha(x,y,t)-\tau_\alpha(x,y,t-\Delta t)}{\Delta t}. \quad (4)$$

As the method is base on FastSim the contact area is discretized with a specific number of elements. This enables to express the temporal and spatial derivatives of $\tau_\alpha(x,y,t)$ in relation to tangential traction in a contiguous element, $\tau_\alpha(x+\Delta x,y,t)$, and in a previous time-step, $\tau_\alpha(x,y,t-\Delta t)$, respectively.

To solve equation(4), it is necessary to give a value to the flexibility parameter, L. For the steady-state rolling contact mechanics, Kalker divided L into three different flexibility parameters [2]; L_1, L_2 and L_3, related to the longitudinal creepage, lateral creepage and spin respectively. These values were determined so that the linear theory is satisfied. Shen and Li used the same three flexibility parameters in the non-steady state method (5), what leads to poor results in some situations [9].

$$\begin{aligned}
\frac{s_x(x,y,t)}{L_s} &= \frac{\xi(t)}{L_1} - \frac{\varphi(t)}{L_3}y - \frac{\tau_x(x+\Delta x,y,t)-\tau_x(x,y,t)}{\Delta x} + \frac{1}{V}\cdot\frac{\tau_x(x,y,t)-\tau_x(x,y,t-\Delta t)}{\Delta t} \\
\frac{s_y(x,y,t)}{L_s} &= \frac{\eta(t)}{L_2} + \frac{\varphi(t)}{L_3}x - \frac{\tau_y(x+\Delta x,y,t)-\tau_y(x,y,t)}{\Delta x} + \frac{1}{V}\cdot\frac{\tau_y(x,y,t)-\tau_y(x,y,t-\Delta t)}{\Delta t},
\end{aligned} \quad (5)$$

where ξ(t), η(t) and φ(t) are the time-dependent longitudinal and lateral creepages and spin respectively. Instead of that, Alonso and Giménez proposed using two different flexibility parameters; L_s, related to the steady state terms and L_v, related to the non-steady state terms.

3.2. *Flexibility parameters of the simplified theory*

The value given to the stationary flexibility coefficient, L_s, is that proposed by Kalker. Thus, when solving a stationary problem, the results are the same as those given by the original FastSim.

The first attempt to determine the dynamic flexibility parameter, L_v, is to follow the same strategy Kalker used to determine the stationary flexibility parameters [2]. This is done expressing L_v as a function of the Kalker's coefficients, C_{ij}.

$$L_v = \chi_{ij}\left(\frac{a}{b}\right)\frac{a}{G\cdot\left(C_{ij}\right)_{\lambda/a\to\infty}} \tag{6}$$

The dimensionless parameters 'χ_{ij}' of are obtained minimizing, for a range of wavelengths, the difference between the non-stationary Linear Theory of Knothe and Groß-Thebing and the non-stationary FastSim of Alonso and Giménez. In the non-stationary Linear Theory the linear relation between forces and creepages, (7), is given by Kalker's non-steady state coefficients $\hat{C}_{ij}$.

$$\begin{aligned} F_x(t) &= -Gab\hat{C}_{11}\hat{\xi}e^{i\omega t} \\ F_y(t) &= -Gab\hat{C}_{22}\hat{\eta}e^{i\omega t} - G\left(ab\right)^{3/2}\hat{C}_{23}\hat{\varphi}e^{i\omega t} \end{aligned} \tag{7}$$

The non-stationary Kalker's coefficients, $\hat{C}_{ij,FS,}$ can be also obtained with the Simpified Theory. For a given creepage, the tangential traction distribution is determined and integrated over the whole contact area to get the contact forces. Once the creepforces are known, the value of $\hat{C}_{ij,FS,}$ can be found from equation (7). The difference between both coefficients, $\hat{C}_{ij}$ and $\hat{C}_{ij,FS}$, is minimized by means of the following function,

$$\Phi\left(\chi_{ij}\right) = \int_{\lambda_{\min}/a}^{\lambda_{\max}/a} \sqrt{\left[\mathrm{Re}(\hat{C}_{ij}) - \mathrm{Re}(\hat{C}_{ij,FS})\right]^2 + \left[\mathrm{Im}(\hat{C}_{ij}) - \mathrm{Im}(\hat{C}_{ij,FS})\right]^2}\, d\left(\frac{\lambda}{a}\right). \tag{8}$$

It is important to remark that the value of 'χ_{ij}' only depends on the ratio between the semi-axes of the contact ellipse as well as the integration limits, here chosen as $(\lambda/a)_{max} = 100$ and $(\lambda/a)_{min} = 1$. The obtained results are tabulated for different ratios between the semi-axes of the contact ellipse, [10]. It is also shown that the results obtained in the validation of the dynamic flexibility parameter are good except for low values of the ratio between the wavelength and the longitudinal semi-axis.

The second attempt consist in adjusting the flexibility parameter by means of a transfer function, which in the frequency-domain adopts the following form,

$$H(\lambda) = \frac{\chi_{ij}^1\cdot\left(a^2/GC_{ij}\right)\cdot i\lambda + \chi_{ij}^2\cdot\left(a^2/GC_{ij}\right)}{\chi_{ij}^3\cdot a\cdot i\lambda + 1}. \tag{9}$$

The form of the filter is chosen so that it does not modify the dependencies between the different parameters involved in the problem. The parameters of the transfer function,' χ_{ij}^k', are determined exactly in the same way as it has been explained for 'χ_{ij}', that is, minimizing $\Phi(\chi_{ij}^k)$. The results are shown in tables 2, 3 and 4 in [10]. As it will be presented below, this solution overcomes the limitations of the first attempt, showing good results in the frequency range of interest.

3.3. *Time integration using FastSim non-stationary algorithm*

During a dynamic simulation of a railway vehicle the creepages do not, necessarily, vary in a sinusoidal form. Thus, the transfer function in the frequency domain is transformed to the time domain. This is done by means of the Z transform:

$$H(z)=\frac{\chi^{1Z}\cdot z^{-1}+\chi^{2Z}}{\chi^{3Z}\cdot z^{-1}+1}. \tag{10}$$

This transfer function of the filter combined with that corresponding to the differentiation operation corresponding to the last terms of equations (4) gives final filter to be used that is expressed by

$$H(z)=\frac{1}{\Delta t}\cdot\frac{-\chi^{1Z}\cdot z^{-2}+(\chi^{1Z}-\chi^{2Z})\cdot z^{-1}+\chi^{2Z}}{\chi^{3Z}\cdot z^{-1}+1}. \tag{11}$$

The time-domain equations (4) transformed to the Z domain become,

$$s_\alpha(x,y,t)=w_\alpha(x,y,t)-L_s\left[\frac{\tau_\alpha(x+\Delta x,y,t)-\tau_\alpha(x,y,t)}{\Delta x}-\frac{1}{V}\cdot H(z)\cdot\tau_\alpha(x,y,t)\right]. \tag{12}$$

FastSim algorithm starts assuming that the contact area is in adhesion, therefore $s_\alpha(x,y,z)=0$. The hypothetical tangential traction distribution should be,

$$\tau_{H\alpha}(x,y,z)=\frac{1}{\left(\frac{H(z)}{V}+\frac{1}{\Delta x}\right)}\cdot\left\{\frac{1}{\Delta x}\cdot\tau_\alpha(x+\Delta x,y,z)-\frac{1}{L_s}\cdot w_\alpha(x,y,z)\right\}. \tag{13}$$

Note that in these expressions variable z does not correspond to a coordinate but to the variable of the Z-transform.

Once the hypothetical tangential traction is known, Coulombs law (2) is used to verify the adhesion assumption.

$$\vec{\tau}(x,y,t)=\begin{cases}\overrightarrow{\tau_H}(x,y,t) & \left|\vec{\tau}(x,y,t)\right|\le\mu P_z(x,y,t)\\ \mu P_z\dfrac{\overrightarrow{\tau_H}(x,y,t)}{\left|\overrightarrow{\tau_H}(x,y,t)\right|} & \left|\vec{\tau}(x,y,t)\right|>\mu P_z(x,y,t)\end{cases} \tag{14}$$

In case the point (x,y) is in adhesion the tangential traction becomes the actual one, however, when it is in the slipping area the tangential traction is limited to the maximum value allowed by the friction law. In that case, it is assumed that both, tangential traction and slip, have the same direction but opposite sense. This process is repeated with all the elements of the contact area in order to obtain the tangential traction distribution. By integrating the latter the wheel-rail contact force at one time step is obtained.

3.4. *Results*

The magnitude and phase of the non-steady Kalker's coefficients, C_{11} and C_{23}, are obtained by means of the non-steady state FastSim and compared to those provided by Knothe and Groß-Thebing.

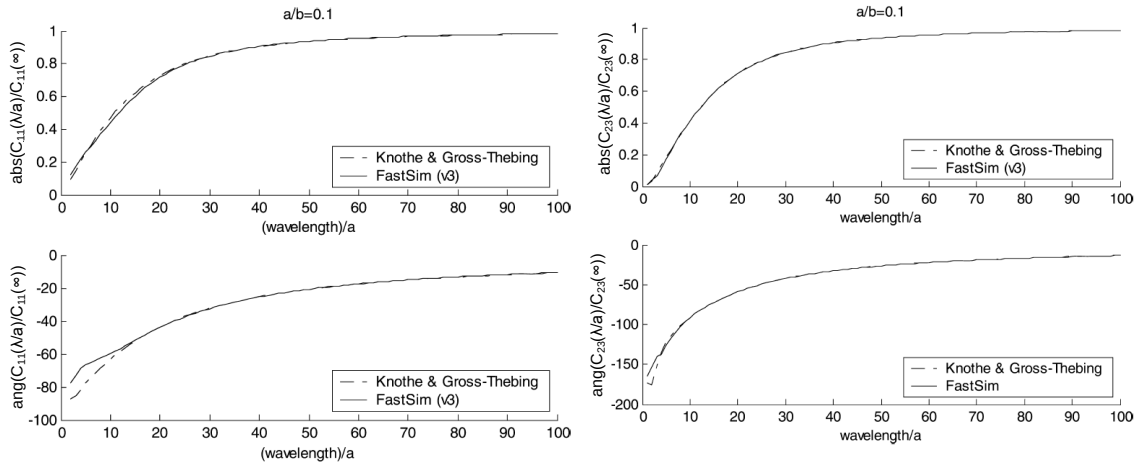

Figure 1. Magnitude and phase of non-steady state Kalker's coefficient vs. the ratio wavelength-longitudinal semi-axis of the contact area, [10].

As shown in Figure 1 the magnitude of the non-stationary Kalker coefficients show good agreement between both theories for any ratio wavelength to contact longitudinal semi-axis. The phase is calculated almost exactly except for cases where the ratio between the wavelength and the longitudinal contact ellipse semi-axis is very low.

Finally, it should be remarked that according to Kalker, non-steady state analysis is necessary in cases in which the ratio $\lambda / a < 10$, however, it can be deduced from Figure 1 that the non-stationary effects become relevant up to about $\lambda / a \approx 50$.

4. Extension of the contact problem theory

Alonso and Giménez took advantage of the success of FastSim among the railway vehicles dynamics software and demonstrated that accurate results can be obtained as soon as the flexibility parameters are recalculated for non-stationary states. However, further work is needed in order to assess the validity of this theory in non-steady state calculations:

- On the one hand, the parameters of the traction function have been obtained assuming that only one creepage varies harmonically with time. Therefore, the way to handle different combinations of creepages was not studied.
- On the other hand, a constant normal load was assumed in all the situations presented in the paper. As it is logical, the normal force can vary with time and therefore the accuracy of the method when solving such situations should be checked. If the normal load varies, the shape and dimensions of the contact area also vary and two different strategies can be followed; the first one consists in remaining constant the dimensions of the mesh which confines the contact, this has some drawbacks though. The second one consists in adapting the mesh to the new dimensions of the contact area at each time step, [12]. The last option improves the results but requires some changes that will be discussed in this section.

4.1. *Arbitrary combination of creepages*

As has been mentioned, the coefficients of the transfer function used to substitute the dynamic flexibility coefficient have been obtained for cases in which only a creepage varies with time significantly. In order to adapt the transfer function for an arbitrary combination of time-varying creepages, the parameters of the transfer function have been adjusted in the following way:

$$\chi_X^{1Z} = \frac{|\xi|\cdot\chi_{11}^{1Z} + |\varphi|\sqrt{ab}\cdot\chi_{23}^{1Z}}{|\xi| + |\varphi|\sqrt{ab}} \qquad \chi_Y^{1Z} = \frac{|\eta|\cdot\chi_{22}^{1Z} + |\varphi|\sqrt{ab}\cdot\chi_{23}^{1Z}}{|\eta| + |\varphi|\sqrt{ab}}$$

$$\chi_X^{2Z} = \frac{|\xi|\cdot\chi_{11}^{2Z} + |\varphi|\sqrt{ab}\cdot\chi_{23}^{2Z}}{\xi + |\varphi|\sqrt{ab}} \qquad \chi_Y^{2Z} = \frac{|\eta|\cdot\chi_{22}^{2Z} + |\varphi|\sqrt{ab}\cdot\chi_{23}^{2Z}}{|\eta| + |\varphi|\sqrt{ab}} \tag{15}$$

$$\chi_X^{3Z} = \frac{|\xi|\cdot\chi_{11}^{3Z} + |\varphi|\sqrt{ab}\cdot\chi_{23}^{3Z}}{|\xi| + |\varphi|\sqrt{ab}} \qquad \chi_Y^{3Z} = \frac{|\eta|\cdot\chi_{22}^{3Z} + |\varphi|\sqrt{ab}\cdot\chi_{23}^{3Z}}{|\eta| + |\varphi|\sqrt{ab}}$$

Note that, although the total number of parameters χ has been reduced from 9 to 6, the number of parameters to be simultaneously identified has been doubled. Instead of having three parameters as in equation (12) , now six parameters have been adopted, three in each direction, x and y. This has been done in order to provide the same results as the original non-steady state FastSim in cases in which only one creepage exists. When a combination of creepages exists the weighted average of the creepages involved in each direction is performed – longitudinal creepage and spin for parameters used in x direction and lateral creepage and spin for parameters used in y direction. The longitudinal and lateral creepages are dimensionless; the spin, however, needs to be adimensionalized by means of the square root of the product of the contact ellipse semi-axes.

The aim of this section is to check the validity of the weighted parameters of the transfer function in equation (15) . Three different combinations of creepages will be studied; small, medium and high variations of creepages.

The first case combines time-dependent lateral and longitudinal creepages. The amplitude is small in order to assure that all the material points of the contact area are in adhesion. Both creepages vary harmonically but have opposite phase. The spin has been given a constant value since it is considered that, in the majority of cases, the variability of this creepage is smaller than it is for the other two creepages.

$$\begin{aligned} \xi(t) &= 0.002\cos(2\pi t / \lambda) \\ \eta(t) &= 0.002\cos(2\pi(t - T/2)/\lambda) \\ \varphi(t) &= 0.0001 \end{aligned} \tag{16}$$

The wavelength, λ, has been chosen in order to get a ratio wavelength to longitudinal semi-axis of $\lambda/a = 15$.

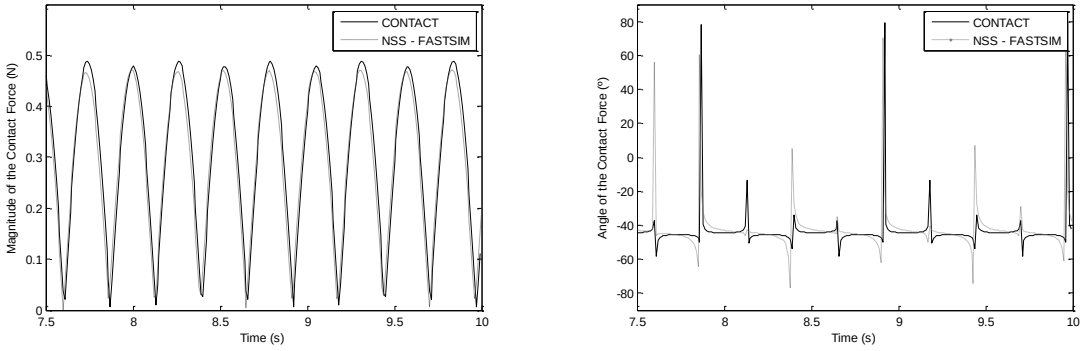

Figure 2. Magnitude and direction of the total force (combination of longitudinal and lateral) using Contact and Non-Steady State FastSim when $\xi = 0.002\cos(2\pi t)$, $\eta = 0.002\cos(2\pi(t-T/2))$ and $\varphi = 0.0001$. The mechanical properties of the material are G = 1MPa, $\upsilon = 0.28$, $\mu = 0.4013$, the normal force is Fzo=470.5 N and V = 25 mm/s.

Figure 2 shows the magnitude and angle of the contact force, both obtained by means of CONTACT and the NSS – FASTSIM (non-steady state FastSim) here presented. The module of the contact force is calculated almost exactly; the angle shows good agreement except for some errors in the peak values. However, these peak values correspond with magnitude values around zero, thus, this error are not significant.

In the second case the amplitude of the creepages has been increased in order to force the emergence of a slip zone,

$$\begin{aligned} \xi(t) &= 0.052\cos(2\pi t / \lambda) \\ \eta(t) &= 0.052\cos(2\pi(t - T/2)/\lambda) \\ \varphi(t) &= 0.001 \end{aligned} \tag{17}$$

The ratio wavelength to longitudinal semi-axis has been decreased to λ/a =10.

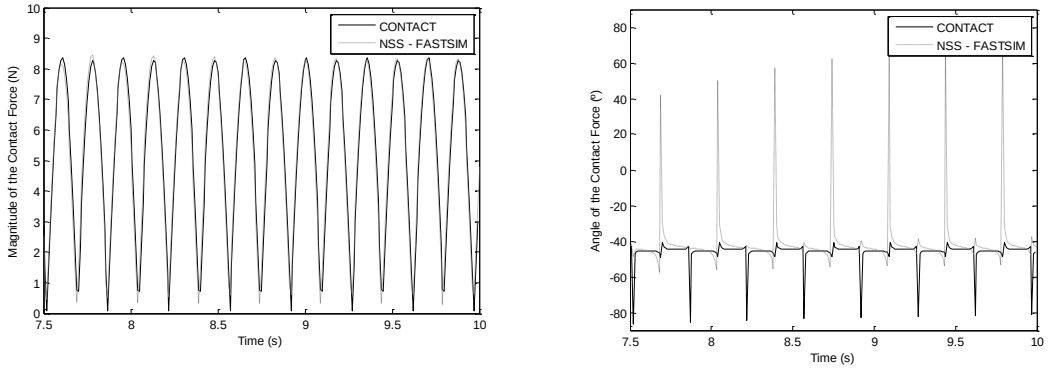

Figure 3. Magnitude and direction of the total force (combination of longitudinal and lateral) using Contact and Non-Steady State FastSim when ξ = 0.052cos(2πt), η=0.052cos(2π(t-0.5)) and φ=0.001. The mechanical properties of the material are G = 1MPa, υ=0.28, μ=0.4013, the normal force is F_{zo}=470.5 N and V = 25 mm/s.

The results (see Figure 3) are similar to those of the previous step; the magnitude of the contact force is calculated almost exactly and the phase shows small errors in the peak amplitudes that are negligible due to the same reason as in the previous case.

The aim of the third case is to check the non-steady state FastSim algorithm when almost all the material points at the contact area are in slip condition. The longitudinal creepage is composed of high constant reference value superimposed to a small harmonic non-stationary component and the lateral creepage is composed of a sinusoidal wave of high amplitude. The spin has been again let constant.

$$\begin{aligned} \xi(t) &= 0.05 + 0.002\cos(2\pi t / \lambda) \\ \eta(t) &= 0.502\cos(2\pi(t - T/2)/\lambda) \\ \varphi(t) &= 0.001 \end{aligned} \tag{18}$$

The ratio wavelength to longitudinal semi-axis has been increased to λ/a =25.

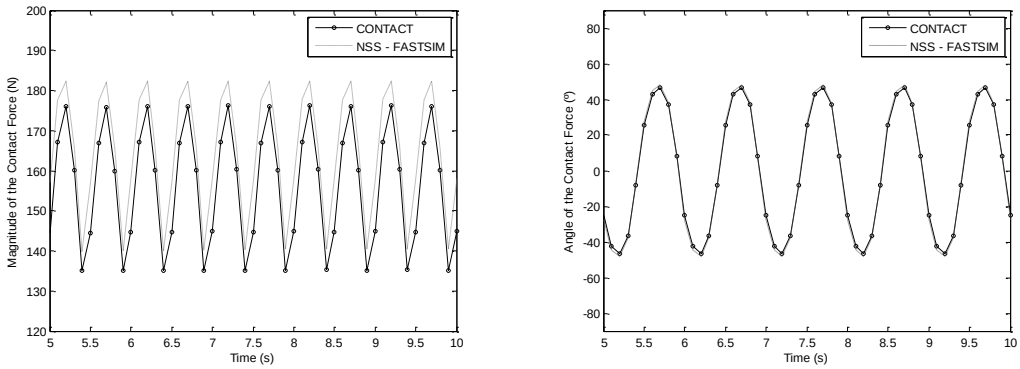

Figure 4. Longitudinal and lateral contact forces using Contact and Non-Steady State FastSim when ξ = 0.05 + 0.002cos(2πt), η=0.502cos(2π(t-0.5)) and φ=0.001. The mechanical properties of the material are G = 1MPa, υ=0.28, μ=0.4013, the normal force is F_{zo}=470.5 N and V = 25 mm/s.

Figure 4 shows good agreement between CONTACT and NSS-FASTSIM as far as magnitude and angle are concerned. There is, however, a small discrepancy in the calculation of the mean value of the contact force which has been confirmed it is given by the stationary FastSim algorithm.

4.2. *Variable normal load*

The size and shape of the contact area are directly related to the value of the normal load. When the latter remains constant the dimensions of the contact area do not change. Thus, the dimensions of the mesh used to discretized the contact path are calculated only once, at the beginning of the simulation, and let constant in the following time-steps. On the contrary, if the normal load varies, the size of the contact area changes. In this case, there are two different ways to proceed:

- The first option is the use of a fixed mesh. The maximum normal load is estimated in order to determine the largest dimensions of the contact area. The dimensions of the mesh are established for that situation. This is the way Kalker's CONTACT [6] discretizes the contact area (see Figure 5). The mesh remains constant the whole simulation.

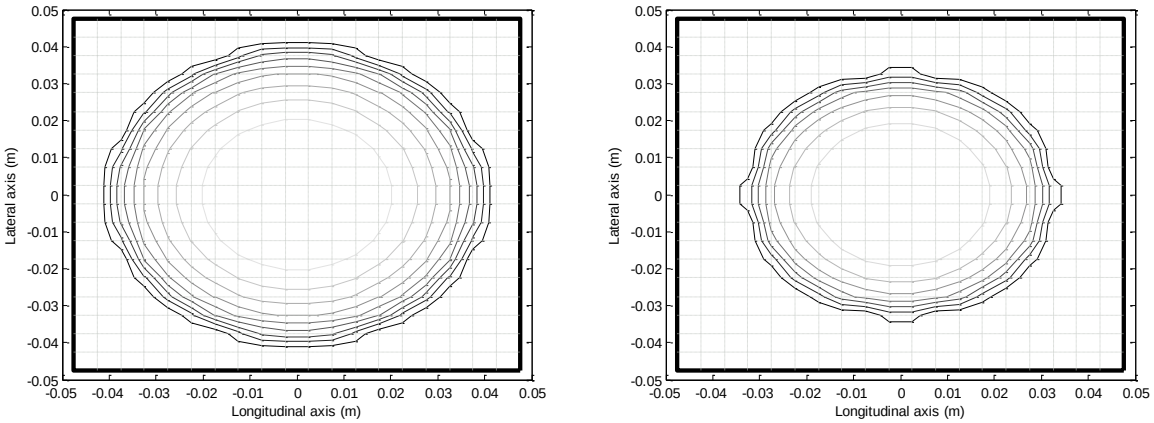

Figure 5. Pressure contour lines of the contact area in two different time-steps (t and t+3Δt) using a fixed mesh.

As stated in equation(12), in non-stationary cases the tangential traction distribution at each time-step depends on its value at previous time-steps. If a fixed mesh is used, the tangential traction value of an element in a previous step can be directly obtained, since the dimensions and the position of the element remain unaltered on the mesh. However, the fixed mesh has a clear drawback. The dimensions of the mesh are calculated based on the less favourable situation – greater normal load. A decay of the normal load implies a reduction of the contact area but, since a fixed discretization is used, the accuracy with which this new area is described decreases. Moreover, in a dynamic simulation the mesh should cover the whole zone in which the contact between both bodies could take place, which demands the mesh to cover a wide zone. This can be avoided, if the number of elements is increased but, this leads to a higher computational cost.

- The second option is the use of an adaptative mesh. The dimensions of the mesh are established based on the dimensions of the contact area, which vary at each time-step (see Figure 6). The mesh is recalculated every time-step.

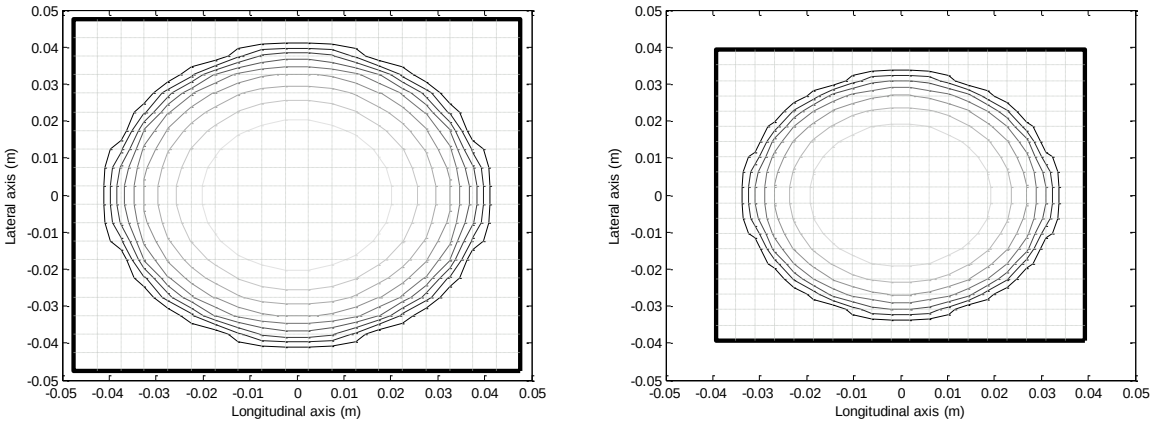

Figure 6. Pressure contour lines of the contact area in two different time-steps (t and t+3Δt) using an adaptative mesh.

The drawbacks of the fixed mesh are overcome if an adaptative mesh is adopted since a resize of the mesh allows maintaining the precision in which the contact area is described (see Figure 6). Nevertheless, the tangential traction distribution at two previous steps must be interpolated in order to adapt its discretization to the new one. The algorithm to perform the interpolations has the following few simple steps:

- Check the contact area in order to identify whether the size/shape has changed.
- For each element, identify the four elements of the previous time-steps that encompass it. The stresses of theses four elements are interpolated by means of the interpolation functions, N_i, used for four-nodes element.

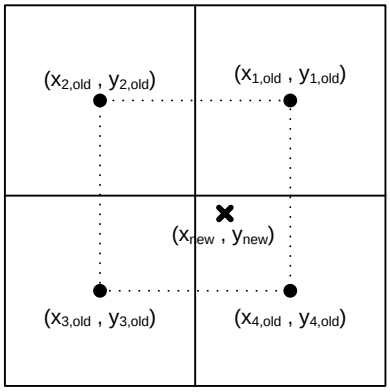

Figure 7. Representation of the remeshing of the contact area.

$$\tau_\alpha(x_{new}, y_{new}) = \sum_{i=1}^{4} N_i \tau_\alpha(x_{old,i}, y_{old,i}), \tag{19}$$

where the interpolation functions satisfy that $N_i(x_{old,i}, y_{old,i}) = 1$ and $N_i(x_{old,j}, y_{old,j}) = 0$ if i≠j.

As can be deduced, with the simple operations carried out in this algorithm, the increment of the computational cost is practically insignificant as long as the accuracy is maintained. The method will be checked for a range of ratio wavelength to longitudinal semi-axis - from λ/a = 0 to λ/a = 75 – and a variable normal force – $F_z = F_{zo}\{1 + 0.25\sin(2\pi t/\lambda)\}$. The longitudinal creepage has been given for different values to check different conditions of the contact area; adhesion (ξ = 0.002), adhesion with slip zones (ξ = 0.01, ξ = 0.05) and slip (ξ = 0.1). The other creepages are zero; η=φ=0.

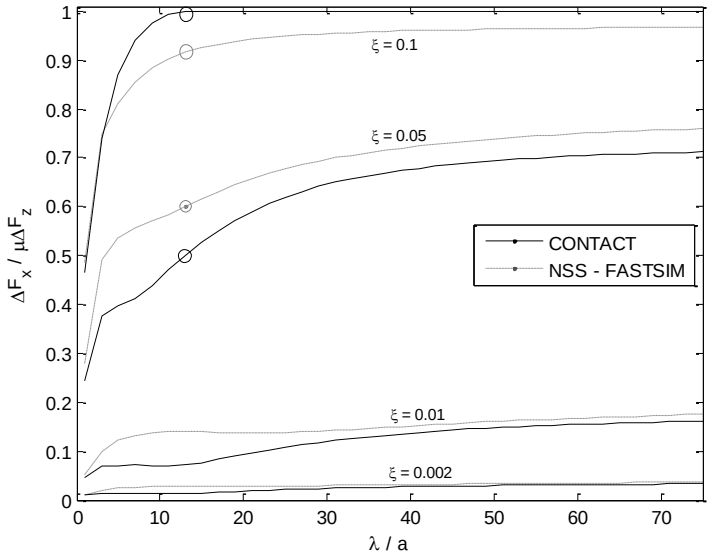

Figure 8. Dimensionless ratio of the peak-to-peak amplitude of the longitudinal non-stationary tangential force for a given λ/a.

The normal load, F_z, varies between $F_{z,\,max} = 1.25F_{zo}$ and $F_{z,min} = 0.75F_z$, thus $\Delta F_z = 0.5\ F_z$. The variation that the longitudinal force suffers between both cases, ΔF_x, is obtained for each λ/a ratio. This value is then divided by $\mu\Delta F_z$ to undimensionalize it. Figure 8 shows acceptable results in the whole range of values of the ratio λ/a. It is worth pointing out that the deviations are given by two sources; the inherent error of the stationary FastSim and the error of the algorithm here presented. It must be also remark that deviations in Figure 8 seem to be higher than they are. This is proven in the following figures (Figure 10 and Figure 9), where the temporal results of two specific points of the curves in Figure 8 are represented.

Figure 9 shows the time-dependent results of the longitudinal and vertical contact forces for λ/a=15 and a longitudinal creepage of 0.05.

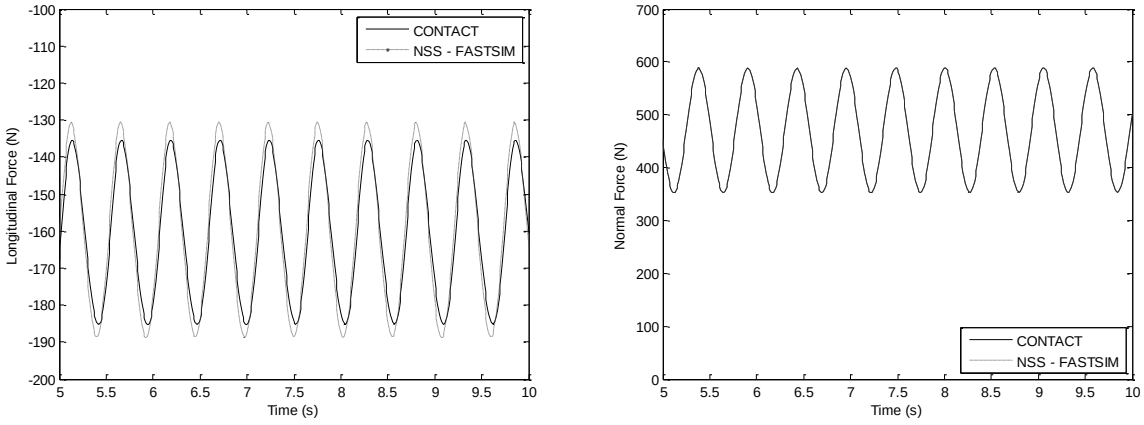

Figure 9. Longitudinal and vertical contact forces for λ/a=15 and ξ = 0.05. The mechanical properties of the material are G = 1MPa, υ=0.28, μ=0.4013, the normal force is F_{zo}=470.5 N and V = 250 mm/s.

Meanwhile the vertical force experiences a variation of 236 N, the longitudinal contact force only varies 50 N. Although Figure 8 showed a deviation at this point, the temporal curves show that the mean value and amplitude are well estimated.

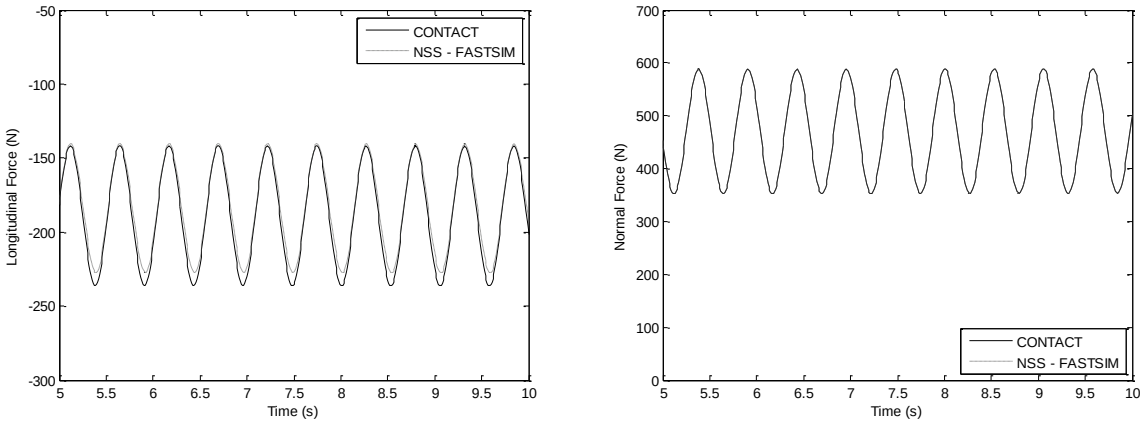

Figure 10. Longitudinal and vertical contact forces for λ/a=15 and ξ = 0.1. The mechanical properties of the material are G = 1MPa, υ=0.28, μ=0.4013, the normal force is F_{zo}=470.5 N and V = 250 mm/s.

In Figure 10 the ratio wavelength to longitudinal semiaxis is maintained as well as the variation of the normal load. The creepage is now given a value of 0.01. The temporal curves also show acceptable results.

5. Conclusions and final remarks

Among all the algorithms Kalker's FastSim has become the most useful computation tool to solve stationary railway simulation problems. However some types of dynamics problems required the use of a non-steady state analysis. Of the existing non-stationary methods, one of the most promising for its use in railway simulation programs is that developed by Alonso and Giménez since it provides sufficiently accurate results with a low computational cost. As it was described in [10] ans [11] it presents some limitations:

- The method was developed for one time-dependent creepage.
- Its accuracy for varying normal forces has not been checked.
- It must be adapted to solve non-hertzian contact areas with an adaptative mesh.

This paper has dealt with the three problems. It has been proven that the use of weighted parameters in the transfer function that substitutes the dynamic flexibility parameter provides good results for an arbitrary combination of creepages. Results have been shown for: a) contact area in adhesion condition, b) contact area in adhesion condition with a small slip zone and, c) contact area in slip condition. Results for different wavelength to longitudinal semi-axis ratio have been obtained; 10, 15 and 25. Finally, for high values of the creepages both types have been checked: a) creepage composed of high constant reference value superimposed to a small harmonic non-stationary component and, b) a creepage composed of a sinusoidal wave of high amplitude.

The validation of the non-stationary FastSim for a varying normal load has been carried out. This has been done for different conditions of the contact zone (adhesion, adhesion-slip, slip) and for a large range of the ratio wavelength to longitudinal semi-axis showing a low correlation between the variable normal load and the tangential force. A way to improve the accuracy of the results is also presented, which consists in the use of an adaptative mesh. This solution allows a more precise description of the contact area maintaining the same computational cost order as FastSim, being the computational time growth of about 5% with respect to the latter.

Finally, although a constant friction coefficient has been assumed, the method can be easily extend to a slip-dependent friction law following [11], [13].

6. References

[1] J. J. Kalker, "On the rolling contact of two elastic bodies in the presence of dry friction," Delft University of Technolgy, 1967.

[2] J. J. Kalker, “A Fast Algorithm for the Simplified Theory of Rolling Contact,” *Vehicle System Dynamics*, vol. 11, pp. 1-13, 1982.

[3] J. J. Kalker, “Transient rolling contact phenomena,” *ASLE Trans*, vol. 14, no. 3, pp. 177-184, 1971.

[4] C. Cattaneo, “Sul Conttato di due corpi elastici: distribuzione locale degli sforci,” *Rendiconti Lincei*, vol. 227, no. 6, pp. 342-348,434-436,474-478, 1875.

[5] F. W. Carter, “On the action of a locomotive driving wheel,” *Proceedings of the Royal Society of London*, vol. 112, no. A, pp. 151-157, 1926.

[6] J. J. Kalker, *Three-Dimensional Elastic Bodies in Rolling Contact*, 1st ed. Dordrecht: Kluwer Academic Publisher, 1990, p. 314.

[7] A. Gross-Thebing, “Frequency-Dependent Creep Coefficients for Three-Dimensional Rolling Contact Problems,” *Vehicle System Dynamics*, vol. 18, no. 6, pp. 359-374, 1989.

[8] A. Gross-Thebing, K. Knothe, and K. Hempelmann, “Wheel-rail contact mechanics for short wavelengths rail irregularities,” *Vehicle System Dynamics*, vol. 20, no. Supl, pp. 210-224, 1991.

[9] Z. Shen and Z. Li, “A fast non-steady state creep force model based on the simplified theory,” *Wear*, vol. 191, no. 1-2, pp. 242-244, Jan. 1996.

[10] A. Alonso and J. G. Giménez, “Non-steady state modelling of wheel-rail contact problem for the dynamic simulation of railway vehicles,” *Vehicle System Dynamics*, vol. 46, no. 3, pp. 179-196, Mar. 2008.

[11] A. Alonso and J. G. Giménez, “Non-steady state contact with falling friction coefficient,” *Vehicle System Dynamics*, vol. 46, no. 908172610, pp. 779-789, 2008.

[12] L. Baeza, F. J. Fuenmayor, J. Carballeira, and A. Roda, “Influence of the wheel-rail contact instationary process on contact parameters,” *Journal of Strain Analysis*, vol. 42, pp. 377-347, 2007.

[13] J. G. Giménez, A. Alonso, and E. Gómez, “Introduction of a friction coefficient dependent on the slip in the FastSim algorithm,” *Vehicle System Dynamics*, vol. 43, no. 4, pp. 233-244, Apr. 2005.